

# Global Optimization with A Power-Transformed Objective and Gaussian Smoothing

Chen Xu<sup>1</sup>

<sup>1</sup>Department of Engineering, Shenzhen MSU-BIT University, China.  
Email: xuchen@smbu.edu.cn

## Abstract

We propose a novel method that solves global optimization problems in two steps: (1) perform a (exponential) power- $N$  transformation to the not-necessarily differentiable objective function  $f$  to obtain  $f_N$ , and (2) optimize the Gaussian-smoothed  $f_N$  with stochastic approximations. Under mild conditions on  $f$ , for any  $\delta > 0$ , we prove that with a sufficiently large power  $N_\delta$ , this method converges to a solution in the  $\delta$ -neighborhood of  $f$ 's global maximum point. The convergence rate is  $O(d^2\sigma^4\varepsilon^{-2})$ , which is faster than both the standard and single-loop homotopy methods. Extensive experiments show that our method requires significantly fewer iterations than other compared algorithms to produce a high-quality solution.

## 1 Introduction

In this work, we consider the global optimization problem of

$$\max_{\mathbf{x} \in \mathcal{S} \subset \mathbb{R}^d} f(\mathbf{x}), \quad (1)$$

where  $f(\mathbf{x})$  is a continuous and non-concave function with a global maximum  $f(\mathbf{x}^*) > \sup_{\mathbf{x} \neq \mathbf{x}^*} f(\mathbf{x})$ , and  $d$  is a positive integer. The minimize-version of this problem is often encountered in machine learning, such as model training and adversarial attack in computer vision. The gradient-based algorithms, such as the (stochastic) gradient descent, are commonly used, which only guarantee to approximate a locally optimal solution in a general case.

Homotopy, also called graduated continuation, is a class of methods for finding a global solution to (1), with many successful applications in machine learning (e.g., []). It converts the original problem to

$$\max_{\boldsymbol{\mu} \in \mathbb{R}^d, \sigma \geq 0} \mathbb{E}_\xi[f(\boldsymbol{\mu} + \sigma\xi)], \quad (2)$$

where  $\sigma \geq 0$  is called the scaling coefficient and  $\xi$  is a random variable with a pre-selected distribution, such as a standard multivariate Gaussian distribution (Gaussian Homotopy, GH) or a uniform distribution in a unit sphere. Based on the observation that  $\boldsymbol{\mu}_\sigma^* := \arg \max_{\boldsymbol{\mu}} \mathbb{E}[f(\boldsymbol{\mu} + \sigma\xi)]$  approaches<sup>1</sup>  $\mathbf{x}^*$  as  $\sigma$  decreases to 0, the homotopy methods admits a double-loop mechanism: the outer loop iteratively decreases  $\sigma$ , and for each fixed value of  $\sigma$ , the inner loop solves  $\max_{\boldsymbol{\mu}} \mathbb{E}[f(\boldsymbol{\mu} + \sigma\xi)]$ , with the solution found in the current inner loop as the starting search point in the next inner loop.

---

<sup>1</sup>Note that  $\mathbb{E}[f(\boldsymbol{\mu} + \sigma\xi)] = f(\boldsymbol{\mu})$  if  $\sigma = 0$ .

The double-loop mechanism of the homotopy methods is costly in time. To tackle this issue, [9] propose a single-loop Gaussian homotopy (SLGH) method that iteratively performs one-step update of  $\boldsymbol{\mu}$  and  $\sigma$ , which reduces the convergence rate from  $O(d^2/\epsilon^4)$  to  $O(d/\epsilon^2)$ . However, in theory SLGH only guarantees to approximate a local optimum<sup>2</sup>, which is not necessarily a global one. A time-efficient algorithm that aims at the global maximum is still to be found.

Therefore, in this work, we propose a new method, namely the Gaussian Smoothing with a Power-transformed Objective (GSPTO), for solving the optimization problem of (1). According to Corollary 1, GSPTO converges to a neighborhood of  $\boldsymbol{x}^*$  with the rate of  $O(d^2\sigma^4/\epsilon^2)$ . It indicates that GSPTO is faster than the standard homotopy and SLGH, if  $\sigma > 0$  is pre-selected to lie in  $(0, 1)$ . This point is verified by experiments in Section 5, which show that the GSPTO-based algorithms (PGS and EPGS, introduced later) are significantly faster than other algorithms to produce high-quality solutions.

## Motivation

Under the condition of  $\int_{\mathbb{R}^d} f(\boldsymbol{x})d\boldsymbol{x} > 0$  and an additional one, there is a threshold  $\sigma_m > 0$  such that whenever  $\sigma > \sigma_m$ , the Gaussian-smoothed objective  $E_{\boldsymbol{\xi} \sim \mathcal{N}(\mathbf{0}, I_d)}[f(\boldsymbol{\mu} + \sigma\boldsymbol{\xi})]$  is concave in  $\boldsymbol{\mu}$  (see [16, Main Result (Corollary 9)]). Hence, Gaussian smoothing converts the original possibly non-concave maximization problem to a concave one, if the maximum point  $\boldsymbol{\mu}^*$  coincides with  $\boldsymbol{x}^*$ . Although this condition is not true in general<sup>3</sup>, we can modify the objective to make  $\boldsymbol{\mu}^*$  close to  $\boldsymbol{x}^*$  (global maximum point of the original objective  $f$  before modification).

Intuitively, if we modify  $f(\boldsymbol{x})$  to put sufficiently large weight on its global maximum  $\boldsymbol{x}^*$ , the global maximum  $\boldsymbol{\mu}^* := \arg \max_{\boldsymbol{\mu}} F(\boldsymbol{\mu}, \sigma)$  should get close enough to  $\boldsymbol{x}^*$ . One way of such modification is by taking powers of  $f$ , if  $f(\boldsymbol{x}^*) > 1$ . The difference  $f^N(\boldsymbol{x}^*) - f^N(\boldsymbol{x})$  is positively related with the power  $N$ , which indicates that more weight is put on  $\boldsymbol{x}^*$  as  $N$  increases. Figure 1 (a) verifies this intuition with an example, and Figure 1(b) illustrates the effects of taking exponential powers.

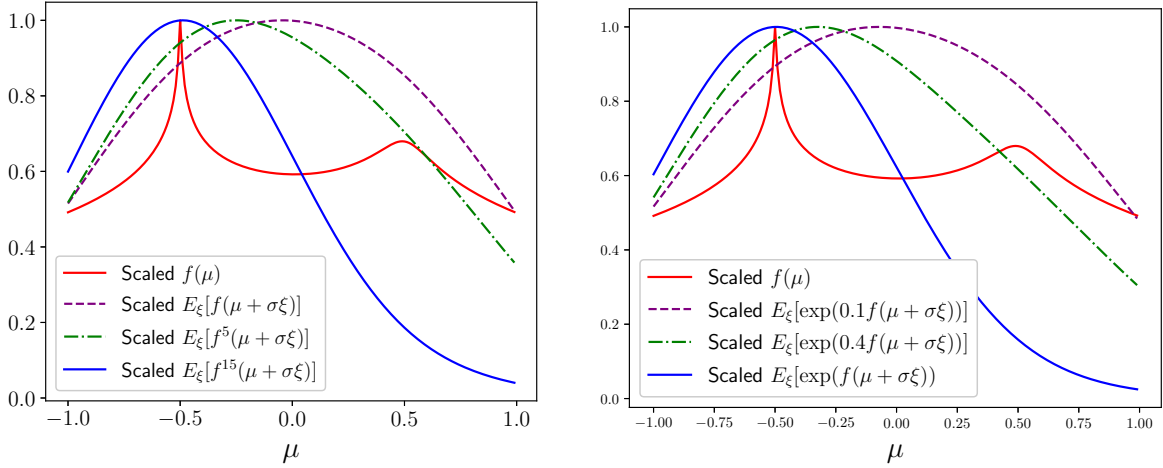
From the above intuition, we propose GSPTO for solving the global optimization problem (1), which is a new method that places more weight on the objective  $f$ 's maximum value (by increasing the gap between the global and local maximum values) before performing Gaussian smoothing. Based on GSPTO, we design two algorithms, Power Gaussian Smoothing (PGS) and Exponential Power Gaussian Smoothing (EPGS), which are featured with replacing the original objective  $f(\boldsymbol{x})$  with a (exponential) power transformation. Specifically, with  $\sigma$  and  $N$  as two hyper-parameters, PGS solves  $\max_{\boldsymbol{\mu}} \mathbb{E}_{\boldsymbol{x} \sim \mathcal{N}(\boldsymbol{\mu}, \sigma^2 I_d)}[f^N(X)]$  and EPGS solves  $\max_{\boldsymbol{\mu}} \mathbb{E}_{\boldsymbol{x} \sim \mathcal{N}(\boldsymbol{\mu}, \sigma^2 I_d)}[e^{Nf(\boldsymbol{x})}]$ , both using a stochastic gradient ascent algorithm derived in this paper, which does not require the differentiability of  $f$ . Here,  $\mathcal{N}$  denotes a multivariate Gaussian distribution and  $I_d$  denotes an identity matrix of dimension  $d \times d$ .

## Related Work

The homotopy methods, firstly proposed in [2, Chapter 7], are intensively studied in the field of machine learning for global optimization problems. [15] derives a bound for the worst scenario of the GH algorithm in a deterministic setting (i.e., the expectation  $\mathbb{E}$  is not approximated with samples), while [8] provides a convergence analysis in a stochastic setting (i.e.,  $\mathbb{E}$  is estimated with samples). Specifically, the latter proves that with a probability

<sup>2</sup>Theorem 4.1 in [9] shows that SLGH approximates a solution  $\hat{\boldsymbol{x}}$  such that  $\mathbb{E}[\nabla f(\hat{\boldsymbol{x}})] = 0$ .

<sup>3</sup>This is why smoothing alone is insufficient for optimization, and is typically used in conjunction with iteratively reducing the scaling parameter, which becomes the homotopy algorithm.



(a) Gaussian Smoothing of  $f^N$ .

(b) Gaussian Smoothing of  $\exp(Nf)$ .

Figure 1: Effects of elevating the objective  $f$  before Gaussian smoothing (A toy example): The maximum point of  $F_N(\mu) := \mathbb{E}_{\xi \sim \mathcal{N}(0,1)}[f_N(\mu + \sigma\xi)]$  gets closer to the global maximum point  $f$  as  $N$  increases, where  $\sigma = 0.5$  and  $f(\mu) = -\log((\mu+0.5)^2 + 10^{-5}) - \log((\mu+0.5)^2 + 10^{-2}) + 10$  for  $|\mu| \leq 1$  and  $f(\mu) = 0$  for  $|\mu| > 1$ . For easier comparison, the graph of each function is scaled to have a maximum value of 1.

greater than  $1 - p$ , the solution  $\hat{\mathbf{x}}$  produced by their proposed homotopy algorithm is  $\epsilon$ -optimal (i.e.,  $f(\mathbf{x}^*) - f(\hat{\mathbf{x}}) < \epsilon$ ) after  $\tilde{O}(d^2/(\sigma^2\epsilon^4))$  steps of solution-update. [6] changes the distribution of the perturbation  $\xi$  from the commonly used Gaussian or uniform to the distribution that minimizes the estimation error of the gradient  $\nabla_{\mu} E_{\xi \sim \mathcal{N}(0, I_d)}[f(\mu + \sigma\xi)]$ . [12] proposes an algorithm for learning the whole solution path produced by the homotopy. Specifically, their algorithm learns a model  $x_{\phi}(\sigma)$  that predicts (for any  $\sigma > 0$ ) the solution to  $\min_{\mu} \nabla_{\mu} E_{\xi \sim \mathcal{N}(0, I_d)}[f(\mu + \sigma\xi)]$ , where  $\phi$  is the set of model parameters to be trained.

The smoothing and homotopy methods have a large number of successful applications in machine learning, such as neural network training ([8]), adversarial attack on image classification models ([9]), solving  $L_1$ -regularized least-square problems ([18]), neural combinatorial optimization ([6]), improving the optimization algorithms of stochastic gradient descent and Adam ([17]), and so on.

There are two existing studies, [5] and [3], that replace the original  $f$  with a surrogate objective,  $\min_{\mu \in \mathcal{C}} G(\mu, \Sigma) := \frac{1}{N} \log(\mathbb{E}_{\xi \sim \mathcal{N}(0, \Sigma)}[e^{Nf(\mu + \xi)}]) + \frac{1}{2}\mu^T R \mu$ , which also involves the exponential transformation  $e^{Nf(\mu + \xi)}$  before smoothing ( $N$  and  $\Sigma$  are pre-selected and fixed). But their works are different from ours. In [5], the proved result<sup>4</sup> that justifies their surrogate objective requires that  $N, R$ , and  $\Sigma$  be selected so that  $NR - \Sigma^{-1}$  is positive semi-definite. This indicates that EPGS, for which  $R = \mathbf{0}$  and  $\Sigma = \sigma I_d$ , is not a special case of theirs, since  $-\sigma I_d$  is negative definite and violates their requirement. Moreover, their theory on the distance between the optimum point of the new surrogate and  $\mathbf{x}^*$  is incomplete (see [5, Section 3.2]). [3] focus on the case where  $N$  is close to 0 (see the sentence below their Eq. (7)), which is very different from GSPTO's requirement that  $N$  is sufficiently large.

## Contribution

This paper introduces a novel method, GSPTO, for solving global optimization problems, with the contributions summarized as follows.

<sup>4</sup> $\min_{\mu} G(\mu, \Sigma)$  is a convex problem given that  $NR - \Sigma^{-1}$  is positive definite and  $\mathcal{C}$  is convex ([5, Theorem 3.1]).

1. To our knowledge, for global optimization problems, this is the first work that proposes the idea<sup>5</sup> of putting more weight on the global maximum values of the objective, to decrease the distance between the optimum point before and after Gaussian smoothing (i.e.,  $\|\mathbf{x}^* - \boldsymbol{\mu}^*\|$ ). PGS and EPGS are two ways of realizing this idea, and future studies are motivated for finding better ones.
2. GSPTO is faster than the homotopy methods (which also apply smoothing) both in theory and practice. According to Corollary 1, GSPTO has a convergence rate of  $O(d^2\sigma^4\varepsilon^{-2})$ , which is faster than the standard homotopy method ( $O(d^2\sigma^{-2}\varepsilon^{-4})$ , [8, Theorem 5.1]), and SLGH ( $O(d^2\varepsilon^{-2})$ , [9, Theorem 4.1]), if  $\sigma$  is pre-selected to lie in  $(0, 1)$ . Extensive experiments show that it is significantly faster than all other compared algorithms (including the homotopy ones) to produce solutions of quality.
3. Our convergence analysis does not require the Lipschitz condition on the original objective  $f$ , which is assumed in the theoretical analysis of homotopy methods in other studies ([8, 9]). Therefore, our analysis applies to more situations.
4. The theory derived in this work is on the distance between the found solution and the optimal one, while the convergence analysis in other studies on homotopy is on the objective value of the found solution. Therefore, our theory has a wider range of applications (e.g., for problems that cares the distance between the found solution and the optimal like inverse problems and adversarial attack in image recognition).

## 2 Preliminaries

We rigorously prove the intuition that motivates PGS and EPGS: Given  $\sigma > 0$ , for any  $\delta > 0$ , there exists a threshold such that whenever  $N$  exceeds this threshold, the global maximum point of  $F_N(\boldsymbol{\mu}, \sigma)$  lies within a  $\delta$ -neighborhood of  $\mathbf{x}^*$ , where  $F_N(\boldsymbol{\mu}) := \mathbb{E}_{\mathbf{x} \sim \mathcal{N}(\boldsymbol{\mu}, \sigma I_d)}[f_N(\mathbf{x})]$ , and

$$\begin{aligned}
 f_N(\mathbf{x}_k) &:= \begin{cases} f^N(\mathbf{x}_k), & \mathbf{x} \in \mathcal{S}; \\ 0, & \text{otherwise,} \end{cases} \quad (\text{PGS setting}); \\
 f_N(\mathbf{x}_k) &:= \begin{cases} e^{Nf(\mathbf{x}_k)}, & \mathbf{x} \in \mathcal{S}; \\ 0, & \text{otherwise.} \end{cases} \quad (\text{EPGS setting}).
 \end{aligned} \tag{3}$$

**Theorem 1.** *Let  $f : \mathcal{S} \subset \mathbb{R}^d \rightarrow \mathbb{R}$  be a continuous function that is possibly non-concave (and non-negative only for the case of PGS), where  $\mathcal{S}$  is compact. Assume that  $f$  has a global maximum  $\mathbf{x}^*$  such that  $\sup_{\mathbf{x}: \|\mathbf{x} - \mathbf{x}^*\| \geq \delta} f(\mathbf{x}) < f(\mathbf{x}^*)$  for any  $\delta > 0$ . For  $\sigma > 0$ , define*

$$F_N(\boldsymbol{\mu}, \sigma) := (\sqrt{2\pi}\sigma)^{-k} \int_{\mathbf{x} \in \mathbb{R}^k} f_N(\mathbf{x}) e^{-\frac{\|\mathbf{x} - \boldsymbol{\mu}\|^2}{2\sigma^2}} d\mathbf{x}, \quad N \in \{0, 1, 2, \dots\},$$

where  $f_N$  is defined in (3) for either PGS or EPGS. Then, for any  $M > 0$  and  $\delta > 0$  such that  $\bar{B}(\mathbf{x}^*; \delta) := \{\mathbf{x} \in \mathbb{R}^d : \|\mathbf{x} - \mathbf{x}^*\| \leq \delta\} \subset \mathcal{S}$ , there exists  $N_{\delta, \sigma, M} > 0$ , such that whenever  $N > N_{\delta, \sigma, M}$ , we have for any  $\|\boldsymbol{\mu}\| < M$  that:  $\frac{\partial F_N(\boldsymbol{\mu}, \sigma)}{\partial \mu_i} > 0$  if  $\mu_i < x_i^* - \delta$ , and  $\frac{\partial F_N(\boldsymbol{\mu}, \sigma)}{\partial \mu_i} < 0$  if  $\mu_i > x_i^* + \delta$ . Here,  $\mu_i$  and  $x_i^*$  denote the  $i^{\text{th}}$  entry of  $\boldsymbol{\mu}$  and  $\mathbf{x}^*$ , respectively, where  $i \in \{1, 2, \dots, d\}$ .

*Proof.* See the appendix for the proof for the EPGS setting. The proof for the PGS setting is similar.  $\square$

---

<sup>5</sup>Although the surrogate objective in [5] can be viewed as a special way of achieving the effect, they have not mentioned this idea.

### 3 Gaussian Smoothing with Power-Transformed Objective

#### 3.1 The Solution Updating Rule

For the optimization problem (1), based on Theorem 1, with the pre-selected hyper-parameters  $N$  and  $\sigma > 0$ , GSPTO follows a stochastic gradient ascent scheme to solve  $\max_{\boldsymbol{\mu}} F_N(\boldsymbol{\mu}, \sigma)$ . Specifically, the rule for updating the solution candidate used is

$$\text{GSPTO : } \quad \boldsymbol{\mu}_{t+1} = \boldsymbol{\mu}_t + \alpha_t \widehat{\nabla F}_N(\boldsymbol{\mu}_t), \quad (4)$$

where  $\widehat{\nabla}_{\boldsymbol{\mu}} F(\boldsymbol{\mu}_t) := \frac{1}{K} \sum_{k=1}^K (\mathbf{x}_k - \boldsymbol{\mu}_k) f_N(\mathbf{x}_k)$ ,  $\{\mathbf{x}_k\}_{k=1}^K$  are independently sampled from the multivariate Gaussian distribution  $\mathcal{N}(\boldsymbol{\mu}, \sigma^2 I_d)$ , and  $f_N(\mathbf{x}_k)$  is defined in (3). Note that  $\widehat{\nabla F}_N(\boldsymbol{\mu}_t)$  is a sample estimate of the gradient  $\nabla F(\boldsymbol{\mu}_t)$ :

$$\begin{aligned} \nabla_{\boldsymbol{\mu}} F(\boldsymbol{\mu}_t) &= \nabla_{\boldsymbol{\mu}} \mathbb{E}_{\mathbf{x} \sim \mathcal{N}(\boldsymbol{\mu}, \sigma^2 I_d)} [f_N(\mathbf{x})] \\ &= (\sqrt{2\pi}\sigma)^{-1} \int_{\mathbf{x} \in B(\mathbf{0}; M)} (\mathbf{x} - \boldsymbol{\mu}_t) f_N(\mathbf{x}) e^{-\frac{\|\mathbf{x} - \boldsymbol{\mu}_t\|^2}{2\sigma^2}} d\mathbf{x}. \\ &= \mathbb{E}_{\mathbf{x} \sim \mathcal{N}(\boldsymbol{\mu}, \sigma I_d)} [(\mathbf{x} - \boldsymbol{\mu}_t) f_N(\mathbf{x})]. \end{aligned}$$

Based on GSPTO, PGS and EPGs are designed in Algorithm 1. They normalize the gradient before updating the solution, which is a common practice to stabilize results.

---

#### Algorithm 1: PGS/EPGS

---

**Require:** The power  $N > 0$ , the scaling parameter  $\sigma > 0$ , the objective  $f$ , the radius  $H$  of the search space (centered at the origin), the initial value  $\boldsymbol{\mu}_0$ , the number  $K$  of sampled points for gradient approximation, the total number  $T$  of  $\boldsymbol{\mu}$ -updates, and the learning rate schedule  $\{\alpha_t\}_{t=1}^T$ .

**Result:**  $\boldsymbol{\mu}_T$  - The approximated solution to (1).

**for**  $t$  from 0 to  $T-1$  **do**

Independently sample from  $\mathcal{N}(\boldsymbol{\mu}_t, \sigma I_d)$  (multivariate Gaussian distribution), and obtain  $\{\mathbf{x}_k\}_{k=1}^K$ .

$\boldsymbol{\mu}_{t+1} = \boldsymbol{\mu}_t + \alpha_t \widehat{\nabla F}_N(\boldsymbol{\mu}_t) / \|\widehat{\nabla F}_N(\boldsymbol{\mu}_t)\|$ , where

$\widehat{\nabla}_{\boldsymbol{\mu}} F(\boldsymbol{\mu}_t) := \frac{1}{K} \sum_{k=1}^K (\mathbf{x}_k - \boldsymbol{\mu}_k) f_N(\mathbf{x}_k)$  and  $f_N(\mathbf{x}_k) := \begin{cases} f^N(\mathbf{x}_k), & \text{for PGS;} \\ e^{Nf(\mathbf{x}_k)}, & \text{for EPGs.} \end{cases}$

**end**

Return( $\boldsymbol{\mu}_T$ ).

---

### 4 Convergence Analysis

We perform convergence analysis for the updating rule (4) under the PGS and EPGs setting (3) on the optimization problem of (1), with  $\mathcal{S} := \{\mathbf{x} \in \mathbb{R}^d : |x_i| \leq M, i \in \{1, 2, \dots, d\}\}$ , for some  $M > 0$ .

We show that, for any  $\varepsilon > 0$  and any  $\delta > 0$ , GSPTO converges to a  $\delta$ -neighborhood of  $\mathbf{x}^*$  with the iteration complexity of  $O(d^2 \sigma^4 \varepsilon^{-2})$ . Specifically, with  $T = O((d\sigma^2)^{2/(1-2\gamma)} \varepsilon^{-2/(1-2\gamma)})$  times of updating  $\boldsymbol{\mu}_t$ ,  $\mathbb{E}[\|\nabla F(\boldsymbol{\mu}_T)\|^2] < \varepsilon$ , where  $\gamma$  can be arbitrarily close to 0. The result is summarized in Corollary 1.

## 4.1 Notation

In this section, let  $\delta > 0$  and  $\sigma > 0$  be fixed, and  $N > 0$  be such that for any  $\|\boldsymbol{\mu}\| \leq \sqrt{d}M$ :  $\frac{\partial F_N(\boldsymbol{\mu}, \sigma)}{\partial \mu_i} > 0$  if  $\mu_i < x_i^* - \delta$ , and  $\frac{\partial F_N(\boldsymbol{\mu}, \sigma)}{\partial \mu_i} < 0$  if  $\mu_i > x_i^* + \delta$ , for all  $i \in \{1, 2, \dots, d\}$ . Such an  $N$  exists because of Theorem 1. Let  $F_N(\boldsymbol{\mu}, \sigma)$  be as defined as in Theorem 1. Unless needed, we omit  $N$  and  $\sigma$  in this symbol as they remain fixed in this section, and write  $F(\boldsymbol{\mu})$  instead.  $\nabla F(\boldsymbol{\mu})$  refers to the gradient of  $F$  with respect to  $\boldsymbol{\mu}$ . Let  $f_N$  be defined as in (3).

## 4.2 Assumptions and Lemmas

**Assumption 1.** Assume that  $f(\mathbf{x})$  is a function satisfying the conditions specified in Theorem 1.

**Assumption 2.** Assume that the learning rate  $\alpha_t$  satisfies

$$\alpha_t > 0, \quad \sum_{t=0}^{\infty} \alpha_t = +\infty, \quad \text{and} \quad \sum_{t=0}^{\infty} \alpha_t^2 < +\infty.$$

**Lemma 1.** Under Assumption 1, any local or global maximum point  $\boldsymbol{\mu}^*$  of  $F(\boldsymbol{\mu})$  belongs to the set of  $\mathcal{S}_{\mathbf{x}^*, \delta} := \{\boldsymbol{\mu} \in \mathbb{R}^d : |\mu_i - x_i^*| \leq \delta, \text{ for each } i \in \{1, 2, \dots, d\}\}$ , where  $i$  denotes the  $i^{\text{th}}$  entry.

*Proof.* For any point  $\boldsymbol{\mu} \notin \mathcal{S}_{\mathbf{x}^*, \delta}$ , we show that  $\nabla F(\boldsymbol{\mu}) \neq 0$ . If  $\boldsymbol{\mu} \in \mathcal{S} - \mathcal{S}_{\mathbf{x}^*, \delta}$ , then  $\|\boldsymbol{\mu}\| \leq \sqrt{d}M$  and there is some  $j \in \{1, 2, \dots, d\}$  such that  $|\mu_j - x_j^*| > \delta$ , which implies  $\frac{\partial F(\boldsymbol{\mu})}{\partial \mu_j} \neq 0$  because of the definition of  $N$  in Section 4.1.

On the other hand, if  $\boldsymbol{\mu} \notin \mathcal{S}$ , there is at least one  $j$  such that  $|\mu_j| > M$ . Then,

$$\begin{aligned} \frac{\partial F(\boldsymbol{\mu})}{\partial \mu_j} &= \frac{1}{(\sqrt{2\pi})^k \sigma^{k+2}} \int_{\mathbf{x} \in \mathbb{R}^d} (x_j - \mu_j) e^{-\frac{\|\mathbf{x} - \boldsymbol{\mu}\|^2}{2\sigma^2}} f_N(\mathbf{x}) d\mathbf{x} \\ &= \frac{1}{(\sqrt{2\pi})^k \sigma^{k+2}} \int_{\mathbf{x} \in \mathcal{S}} (x_j - \mu_j) e^{-\frac{\|\mathbf{x} - \boldsymbol{\mu}\|^2}{2\sigma^2}} f_N(\mathbf{x}) d\mathbf{x}, \text{ by def. of } f_N \text{ in (3),} \\ &= \begin{cases} \text{negative,} & \text{if } \mu_j > M; \\ \text{positive,} & \text{if } \mu_j < -M. \end{cases}, \text{ since } x_j \in \mathcal{S} \Rightarrow |x_j| \leq M \text{ by Def of } \mathcal{S}. \end{aligned}$$

In sum, for any point  $\boldsymbol{\mu} \notin \mathcal{S}_{\mathbf{x}^*, \delta}$ ,  $\nabla F(\boldsymbol{\mu}) \neq 0$ , which further implies that any local or global maximum point  $\boldsymbol{\mu}^*$  of  $F(\boldsymbol{\mu})$  belongs to  $\mathcal{S}_{\mathbf{x}^*, \delta}$  since  $\nabla F(\boldsymbol{\mu}^*) = 0$ .  $\square$

**Lemma 2.** Under Assumption 1, for any  $\sigma > 0$ , the objective function  $F_N(\boldsymbol{\mu}, \sigma)$  is Lipschitz Smooth. That is, for any  $\boldsymbol{\mu}_1, \boldsymbol{\mu}_2 \in \mathbb{R}^d$ ,

$$\|\nabla F(\boldsymbol{\mu}_1, \sigma) - \nabla F(\boldsymbol{\mu}_2, \sigma)\| \leq L \|\boldsymbol{\mu}_1 - \boldsymbol{\mu}_2\|,$$

where  $L = f^N(\mathbf{x}^*)$  for the case of PGS and  $L = e^{Nf(\mathbf{x}^*)}$  for the case of EPGS.

*Proof.*  $F_N(\boldsymbol{\mu}, \sigma) = \mathbb{E}_{\mathbf{x} \sim \mathcal{N}(\boldsymbol{\mu}, \sigma^2 I_d)}[f_N(\mathbf{x})]$ , where  $f_N(\mathbf{x})$  is as defined in (3).  $\nabla_{\boldsymbol{\mu}} F(\boldsymbol{\mu}, \sigma) = \mathbb{E}_{\mathbf{x} \sim \mathcal{N}(\boldsymbol{\mu}, \sigma^2 I_d)}[(\mathbf{x} - \boldsymbol{\mu}) f_N(\mathbf{x})]$ . Then,

$$\|\nabla F(\boldsymbol{\mu}_1, \sigma) - \nabla F(\boldsymbol{\mu}_2, \sigma)\| = \|\mathbb{E}_{\mathbf{x} \sim \mathcal{N}(\boldsymbol{\mu}, \sigma^2 I_d)}[(\boldsymbol{\mu}_1 - \boldsymbol{\mu}_2) f_N(\mathbf{x})]\| \leq \|\boldsymbol{\mu}_1 - \boldsymbol{\mu}_2\| f_N(\mathbf{x}^*).$$

Hence,  $L = f_N(\mathbf{x}^*)$ , which is  $f^N(\mathbf{x}^*)$  for PGS and  $L = e^{Nf(\mathbf{x}^*)}$  for EPGS.  $\square$

**Lemma 3.** Under Assumption 1, for any  $\sigma > 0$ , let  $\hat{\nabla}_{\boldsymbol{\mu}} F_N(\boldsymbol{\mu}, \sigma)$  be as defined in Algorithm 1. Then,  $\mathbb{E}[\|\hat{\nabla}_{\boldsymbol{\mu}} F_N(\boldsymbol{\mu}, \sigma)\|^2] < G$ , where

$$\begin{aligned} G &= d\sigma^2 f^{2N}(\mathbf{x}^*), & \text{for PGS;} \\ G &= d\sigma^2 e^{2Nf(\mathbf{x}^*)}, & \text{for EPGS.} \end{aligned}$$

*Proof.* For the case of EPGS,

$$\begin{aligned} \mathbb{E} \left[ \|\hat{\nabla} F_N(\boldsymbol{\mu}_t)\|^2 \right] &= \frac{1}{K^2} \sum_{k=1}^K \sum_{l=1}^K \mathbb{E}_{\mathbf{x}_k, \mathbf{x}_l \sim \mathcal{N}(\boldsymbol{\mu}_t, \sigma^2 I_d)} [(\mathbf{x}_k - \boldsymbol{\mu}_t)'(\mathbf{x}_l - \boldsymbol{\mu}_t) f_N(\mathbf{x}_k) f_N(\mathbf{x}_l)] \\ &\leq f_N^2(\mathbf{x}^*) \frac{1}{K^2} \sum_{k=1}^K \sum_{l=1}^K \mathbb{E}_{\mathbf{x}_k, \mathbf{x}_l \sim \mathcal{N}(\boldsymbol{\mu}_t, \sigma^2 I_d)} [ |(\mathbf{x}_k - \boldsymbol{\mu}_t)'(\mathbf{x}_l - \boldsymbol{\mu}_t)| ] \\ &\leq f_N^2(\mathbf{x}^*) \frac{1}{K^2} \sum_{k=1}^K \sum_{l=1}^K \mathbb{E}_{\mathbf{x}_k, \mathbf{x}_l \sim \mathcal{N}(\boldsymbol{\mu}_t, \sigma^2 I_d)} [ \|(\mathbf{x}_k - \boldsymbol{\mu}_t)\| \cdot \|(\mathbf{x}_l - \boldsymbol{\mu}_t)\| ], \\ &\leq f_N^2(\mathbf{x}^*) \frac{1}{K^2} \sum_{k=1}^K \sum_{l=1}^K \sqrt{\mathbb{E}[\|\mathbf{x}_k - \boldsymbol{\mu}_t\|^2] \mathbb{E}[\|\mathbf{x}_l - \boldsymbol{\mu}_t\|^2]}, \quad \text{by Schwarz Ineq.,} \\ &= f_N^2(\mathbf{x}^*) d\sigma^2, \quad d \text{ denotes number of dimensions,} \end{aligned}$$

where the third line is by Cauchy-Schwarz Inequality. Replacing  $f_N^2(\mathbf{x}^*) = e^{2Nf(\mathbf{x}^*)}$  for EPGS and  $f_N^2(\mathbf{x}^*) = f^{2N}(\mathbf{x}^*)$  for PGS.  $\square$

### 4.3 Convergence Rate

**Theorem 2.** Let  $\{\boldsymbol{\mu}_t\}_{t=0}^T \subset \mathbb{R}^d$  be produced by following the iteration rule of (4), with a pre-selected and deterministic  $\boldsymbol{\mu}_0$  and all the involved terms defined as in Section 4.1. Then, under Assumption 1 and 2, we have that

$$\sum_{t=0}^{T-1} \alpha_t \mathbb{E}[\|\nabla F(\boldsymbol{\mu}_t)\|^2] \leq f(\mathbf{x}^*) - F(\boldsymbol{\mu}_0) + LG \sum_{t=1}^{\infty} \alpha_t^2,$$

where  $G = d\sigma^2 f^{2N}(\mathbf{x}^*)$  under the PGS setting and  $G = d\sigma^2 e^{2Nf(\mathbf{x}^*)}$  under the EPGS setting.

**Remark 1.** If  $\alpha_t = (t+1)^{-(1/2+\gamma)}$  with  $\gamma \in (0, 1/2)$ . Then,

$$\frac{f(\mathbf{x}^*) - F(\boldsymbol{\mu}_0) + LG \sum_{t=1}^{\infty} t^{-(1+2\gamma)}}{\sum_{t=1}^T t^{-(1/2+\gamma)}} < \frac{f(\mathbf{x}^*) - F(\boldsymbol{\mu}_0) + LG \sum_{t=1}^{\infty} t^{-(1+2\gamma)}}{\int_1^T t^{-(1/2+\gamma)} dt} = O(d\sigma^2 T^{-1/2+\gamma}).$$

This inequality and Theorem 2 implies that after  $T = O((d\sigma^2 \varepsilon^{-1})^{2/(1-2\gamma)})$  times of updating  $\boldsymbol{\mu}_t$  by GSPTO,  $\mathbb{E}[\|\nabla F(\boldsymbol{\mu}_T)\|^2] < \varepsilon$ . In sum, the GSPTO method (4) converges to a  $\delta$ -neighborhood of  $\mathbf{x}^*$  with a rate of  $O((d\sigma^2 \varepsilon^{-1})^{2/(1-2\gamma)})$ , where  $\gamma$  can be arbitrarily close to 0.

*Proof.* By the Gradient Mean Value Theorem, there exists  $\boldsymbol{\nu}_t \in \mathbb{R}^d$  such that for each of the  $i$ th entry  $\nu_{t,i}$  lies between  $\mu_{t+1,i}$  and  $\mu_{t,i}$ , and

$$\begin{aligned} F(\boldsymbol{\mu}_{t+1}) &= F(\boldsymbol{\mu}_t) + (\nabla F(\boldsymbol{\nu}_t))'(\boldsymbol{\mu}_{t+1} - \boldsymbol{\mu}_t), \quad ' \text{ denotes matrix transpose,} \\ &= F(\boldsymbol{\mu}_t) + (\nabla F(\boldsymbol{\mu}_t))'(\boldsymbol{\mu}_{t+1} - \boldsymbol{\mu}_t) + (\nabla F(\boldsymbol{\nu}_t) - \nabla F(\boldsymbol{\mu}_t))'(\boldsymbol{\mu}_{t+1} - \boldsymbol{\mu}_t) \\ &= F(\boldsymbol{\mu}_t) + \alpha_t (\nabla F(\boldsymbol{\mu}_t))'(\hat{\nabla} F(\boldsymbol{\mu}_t)) - (\nabla F(\boldsymbol{\mu}_t) - \nabla F(\boldsymbol{\nu}_t))'(\boldsymbol{\mu}_{t+1} - \boldsymbol{\mu}_t) \\ &\geq F(\boldsymbol{\mu}_t) + \alpha_t (\nabla F(\boldsymbol{\mu}_t))'(\hat{\nabla} F(\boldsymbol{\mu}_t)) - L \|\boldsymbol{\nu}_t - \boldsymbol{\mu}_t\| \cdot \|\boldsymbol{\mu}_{t+1} - \boldsymbol{\mu}_t\|, \quad \text{by Lemma 2,} \\ &\geq F(\boldsymbol{\mu}_t) + \alpha_t (\nabla F(\boldsymbol{\mu}_t))'(\hat{\nabla} F(\boldsymbol{\mu}_t)) - L \|\boldsymbol{\mu}_{t+1} - \boldsymbol{\mu}_t\|^2, \quad \nu_{t,i} \text{ is between } \mu_{t+1,i} \text{ and } \mu_{t,i} \\ &\geq F(\boldsymbol{\mu}_t) + \alpha_t (\nabla F(\boldsymbol{\mu}_t))'(\hat{\nabla} F(\boldsymbol{\mu}_t)) - \alpha_t^2 L \|\hat{\nabla} F_N(\boldsymbol{\mu}_t)\|^2. \end{aligned}$$

Hence, we have

$$F(\boldsymbol{\mu}_{t+1}) \geq F(\boldsymbol{\mu}_t) + \alpha_t (\nabla F(\boldsymbol{\mu}_t))' (\hat{\nabla} F(\boldsymbol{\mu}_t)) - \alpha_t^2 L \|\hat{\nabla} F_N(\boldsymbol{\mu}_t)\|^2.$$

Taking the expectation of both sides gives

$$\begin{aligned} \mathbb{E}[F(\boldsymbol{\mu}_{t+1})] &\geq \mathbb{E}[F(\boldsymbol{\mu}_t)] + \alpha_t \mathbb{E}[\|\nabla F(\boldsymbol{\mu}_t)\|^2] - \alpha_t^2 L \mathbb{E}[\|\hat{\nabla} F_N(\boldsymbol{\mu}_t)\|^2] \\ &\geq \mathbb{E}[F(\boldsymbol{\mu}_t)] + \alpha_t \mathbb{E}[\|\nabla F(\boldsymbol{\mu}_t)\|^2] - \alpha_t^2 LG, \text{ by Lemma 3,} \end{aligned} \quad (5)$$

where for the first line, note that

$$\mathbb{E}[(\nabla F(\boldsymbol{\mu}_t))' (\hat{\nabla} F(\boldsymbol{\mu}_t))] = \mathbb{E} \left[ \mathbb{E}[(\nabla F(\boldsymbol{\mu}_t))' (\hat{\nabla} F(\boldsymbol{\mu}_t)) | \boldsymbol{\mu}_t] \right] = \mathbb{E}[\|\nabla F(\boldsymbol{\mu}_t)\|^2].$$

Taking the sum from  $t = 0$  to  $t = T - 1$  on both sides of (5) gives

$$\mathbb{E}[F(\boldsymbol{\mu}_T)] \geq \mathbb{E}[F(\boldsymbol{\mu}_0)] + \sum_{t=0}^{T-1} \alpha_t \mathbb{E}[\|\nabla F(\boldsymbol{\mu}_t)\|^2] - LG \sum_{t=0}^{T-1} \alpha_t^2.$$

Re-organizing the terms gives

$$\begin{aligned} \sum_{t=0}^{T-1} \alpha_t \mathbb{E}[\|\nabla F(\boldsymbol{\mu}_t)\|^2] &\leq \mathbb{E}[F(\boldsymbol{\mu}_T)] - \mathbb{E}[F(\boldsymbol{\mu}_0)] + LG \sum_{t=0}^{T-1} \alpha_t^2 \\ &\leq f(\mathbf{x}^*) - F(\boldsymbol{\mu}_0) + LG \sum_{t=0}^{\infty} \alpha_t^2 \end{aligned}$$

□

We summarize the above results in the following corollary.

**Corollary 1.** *Suppose Assumption 1 and 2 hold. Given any  $\delta > 0$  and  $\sigma > 0$ , there exists  $N > 0$  such that  $F_N(\boldsymbol{\mu})$  has all its local maximums in  $\mathcal{S}_{\mathbf{x}^*, \delta} := \{\boldsymbol{\mu} \in \mathbb{R}^d : |\mu_i - x_i^*| \leq \delta, \text{ for each } i \in \{1, 2, \dots, d\}\}$ . For any  $\varepsilon > 0$ , under either the PGS or EPGS setting, the updating rule (4) of GSPTO produces  $\boldsymbol{\mu}_t$  that converges to a local maximum point of  $F_N(\boldsymbol{\mu})$ , which lies in a  $\delta$ -neighborhood of  $\mathbf{x}^*$ , with the iteration complexity of  $O(d^2 \sigma^4 \varepsilon^{-2})$ . Specifically, after  $T = O((d\sigma^2 \varepsilon^{-1})^{2/(1-2\gamma)})$  times of  $\boldsymbol{\mu}_t$ -updating by (4),  $\mathbb{E}[\|\nabla F(\boldsymbol{\mu}_T)\|^2] < \varepsilon$ , where  $\gamma \in (0, 1/2)$  is a parameter in the learning rate  $\alpha_t := (t + 1)^{-(1/2+\gamma)}$  and can be arbitrarily close to 0.*

## 5 Experiments

### 5.1 Effects of Increasing Powers

We illustrate the improvements made by increasing  $N$  for PGS/EPGS through an example problem of

$$\max_{\mathbf{x} \in \mathbb{R}^d} f(\mathbf{x}) := -\log(\|\mathbf{x} - \mathbf{m}_1\|^2 + 10^{-5}) - \log(\|\mathbf{x} - \mathbf{m}_2\|^2 + 10^{-2}), \quad (6)$$

the global maximum point  $\mathbf{m}_1 \in \mathbb{R}^d$  has all its entries equal to  $-0.5$ , and the local maximum point  $\mathbf{m}_2 \in \mathbb{R}^d$  has all its entries equal to  $0.5$ . The graph of its 2D-version is plotted in Figure 2.

With each value of  $N$ , both the PGS and EGS are performed to solve this problem. The  $N$ -candidate set is  $\{10, 20, \dots, 65\}$  for PGS and  $\{1.0, 1.5, 2.0, \dots, 4.5\}$  for EGS. For each



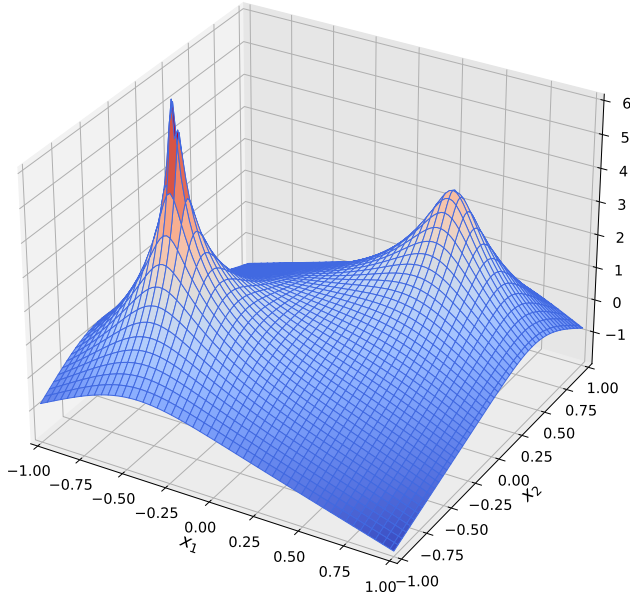


Figure 2:  $f(\mathbf{x}) = -\log(\|\mathbf{x} - \mathbf{m}_1\|^2 + 10^{-5}) - \log(\|\mathbf{x} - \mathbf{m}_2\|^2 + 10^{-2})$

$N$  value, we do 100 trials to stabilize the result. In each trial, the initial solution candidate  $\boldsymbol{\mu}_0$  is uniformly sampled from  $C := \{\mathbf{x} \in \mathbb{R}^d | x_i \in [-1.0, 1.0], i \in \{1, 2, \dots, d\}\}$ , where  $x_i$  represents the  $i^{\text{th}}$  entry of  $\mathbf{x}$ . We set the initial learning rate as 0.1, the scaling parameter  $\sigma$  is set as 0.5, and the total number of solution updates as 1000. The objective for Power-GS is modified to be  $f_1(\mathbf{x}) := f(\mathbf{x}) + 10$  to ensure that the PGS agent will not encounter negative fitness values during the 1000 steps.

We perform the experiments in two settings, one is two-dimensional ( $d = 2$ ) and the other is five-dimensional ( $d = 5$ ). The results, plotted in Figure 3, show that, as  $N$  increases, the distance between the produced solution  $\boldsymbol{\mu}^*$  and the global maximum point  $\mathbf{x}^*$  approaches zero (see the decreasing MSE curve in the plot), which is consistent with Theorem 1 and the idea that  $F(\boldsymbol{\mu})$ 's maximum  $\boldsymbol{\mu}^*$  approaches the global maximum point  $\mathbf{x}^*$  of  $f$  as we put more weight on  $f(\mathbf{x}^*)$

## 5.2 Performance on Benchmark Objective Functions

In this subsection, we test the performance of PGS and EGS on two popular benchmark objective functions, the Ackley and the Rosenbrock (max-version). The performances of other popular global algorithms (max-version) are also reported for comparison, including a standard homotopy method STD-Homotopy, ZO-SLGHd and ZO-SLGHr ([9]), the algorithms of ZO-SGD ([7]) and ZO-AdaMM([4]) for solving  $\min_{\mathbf{x}} \mathbb{E}_{\xi}[f(\mathbf{x}) + \xi]$ , as well as the evolutionary algorithm of particle swarm optimization (PSO, e.g., [13, Section 3.1.5] and [14]). The hyper-parameters of these algorithms are selected by trials, and the optimal ones can be found in our codes at <http://github.com/chen-research/GS-PowerTransform>.

### 5.2.1 Ackley

The Ackley objective function features with a numerous number of local optimums and a single global optimum. We solve the max-version of the corresponding problem, which is

$$\max_{(x,y) \in \mathbb{R}^2} f(x,y) := 20e^{-0.2\sqrt{0.5(x^2+y^2)}} + e^{0.5(\cos(2\pi x) + \cos(2\pi y))}.$$

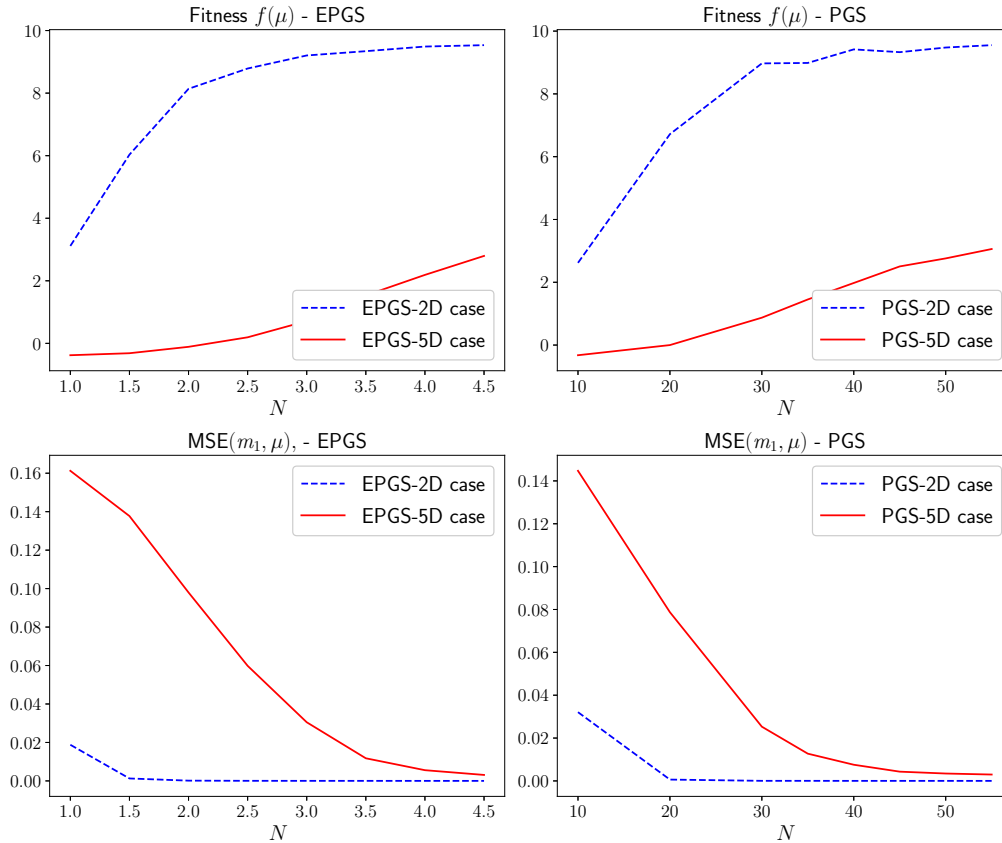


Figure 3: Effects of Increasing  $N$ . For each  $N$ , we perform the algorithm 100 times and obtain  $\{\mu_k\}_{k=1}^{100}$ . The average fitness  $\sum_{k=1}^{100} f(\mu_k)/100$  and  $\sum_{k=1}^{100} MSE(m_1, \mu_k)/100$  are plotted, where  $MSE(m_1, \mu_k) := \sum_{i=1}^d (\mu_{ki} + 0.5)^2/d$ ,  $\sigma = 1.0$ , and  $f$  is defined in 6.

The graph of this function is plotted in Figure 4(a). From both the functional form and the graph, it is not difficult to see that  $f(x, y)$  attains its maximum at  $(0, 0)$ .

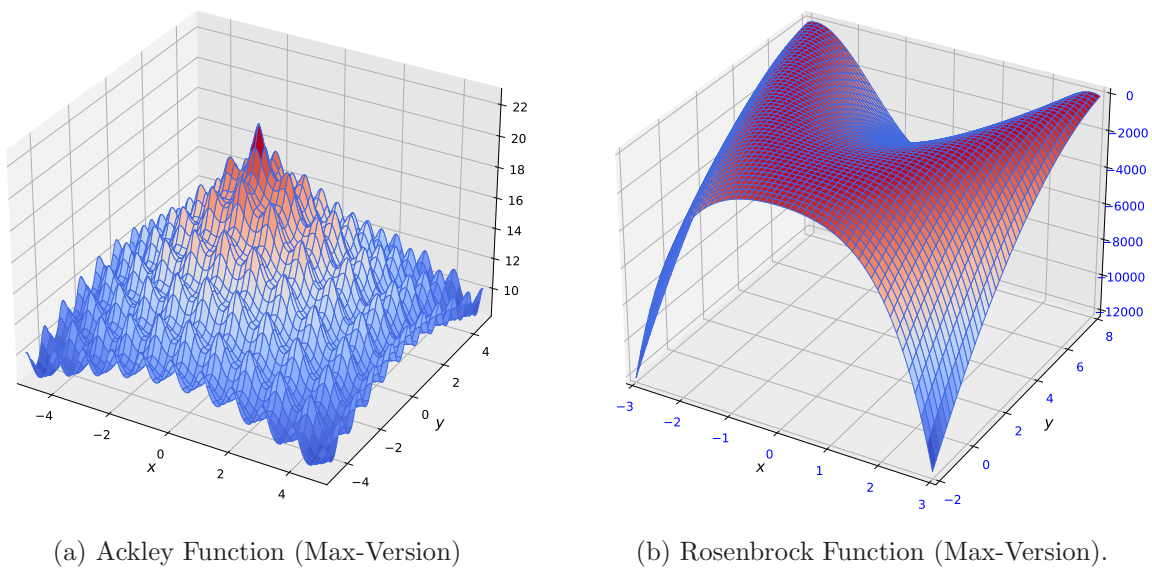


Figure 4: Graph of objective functions.

The solutions and their fitness values found by each of the compared algorithms are reported in Table 1. From which we see that all of these algorithms are able to avoid the

local maximum points and achieve the global maximum point.

Table 1: Performances on Maximizing Ackley. The limit of the number of iterations is set as 3000, and 100 samples are used for each solution update. The initial solution value is set as  $\boldsymbol{\mu}_0 := [5.0, 5.0]$ , except for PSO. For PSO, the initial population is sampled from a multivariate Gaussian with mean  $\boldsymbol{\mu}_0$  and covariance  $\sigma^2 I_2$ , with  $\sigma = 0.01$  for PSO1 and  $\sigma = 1.0$  for PSO2. In the table, ‘‘Iterations Taken’’ refers to the number of iterations taken to reach the best found solution. The hyper-parameters are selected by trials. All numbers are rounded to keep 3 decimal places. The global maximum point of the Ackley function is (0,0).

	Iterations Taken	Best Solution Found ( $\boldsymbol{\mu}^*$ )	$f(\boldsymbol{\mu}^*)$
EPGS ( $N = 3$ )	622.	(0.0, 0.0)	22.715
PGS ( $N = 10$ )	476	(0.001, 0.0)	22.717
STD-Homotopy	2340	(0.003, 0.0)	22.708
ZO-SLGHD	699	(−0.001, 0.0).	22.714
ZO-SLGHr	711	(−0.003, −0.004).	22.704
ZO-AdaMM	688	(0.002, 0.0).	22.713
ZO-SGD	1736	(−0.002, 0.002).	22.710
PSO1	-	(4.983, 3.987).	10.817
PSO2	-	(0.0, 0.0).	22.718

### 5.2.2 Rosenbrock

The Rosenbrock objective is known to be difficult to optimize, since its global optimum point  $\boldsymbol{x}^* = (1.0, 1.0)$  is surrounded by a flat curved plane (see Figure). Specifically, the problem to be solved is  $\max_{(x,y) \in \mathbb{R}^2} f(x, y)$ , where

$$f(x, y) = -100(y - x^2)^2 - (1 - x)^2.$$

We use PGS, EPGS, and other algorithms to solve  $\max_{\boldsymbol{x}} f(\boldsymbol{x})$ . Their performances are recorded in Table 2, which shows that EPGS, STD-Homotopy, and PSO are superior than other algorithms on this task, since they are able to locate the true solution of (1,1).

### 5.2.3 Conclusions on Algorithm Performances for Benchmark Objectives

For Ackley, all the algorithms are able to locate the true solution of (1,1), except PSO when the initial population is concentrated near the initial start of  $\boldsymbol{\mu}_0$ , which indicates that the performance of PSO depends more on the initial guess than other methods. For Rosenbrock, EPGS is one of the three algorithms that can locate the global optimum well.

## 5.3 Performance on the Black-box Targeted Adversarial Attack

Let  $\mathcal{C}$  be an black-box<sup>6</sup> image classifier. The targeted adversarial attack on  $\mathcal{C}$  refers to the task of modifying the pixels of a given image  $\boldsymbol{a}$  so that  $\mathcal{C}(\boldsymbol{a} + \boldsymbol{x})$  is equal to a pre-specified target label  $\mathcal{T}$ , where  $\boldsymbol{x}$  denotes the perturbation and  $\mathcal{T} \neq \mathcal{C}(\boldsymbol{a})$ . Another goal of this task is to minimize the modification  $\|\boldsymbol{x}\|$ . Hence, I set the loss as

$$L(\boldsymbol{x}) := \max_{i \neq \mathcal{T}} (\max \mathcal{C}(\boldsymbol{a} + \boldsymbol{x})_i - \mathcal{C}(\boldsymbol{a} + \boldsymbol{x})_{\mathcal{T}}, \kappa) + \lambda \|\boldsymbol{x}\|,$$

<sup>6</sup>A black-box classifier refers to a classification model whose parameters are not accessible.

Table 2: Performances on Maximizing Rosenbrock. The limit of the number of iterations is set as 3000, and 100 samples are used for each solution update. The initial solution value is set as  $\boldsymbol{\mu}_0 := [5.0, 5.0]$ , except for PSO. For PSO, the initial population is sampled from a multivariate Gaussian with mean  $\boldsymbol{\mu}_0$  and covariance  $\sigma^2 I_2$ , with  $\sigma = 0.01$ . In the table, “Iterations Taken” refers to the number of iterations taken to reach the best found solution. The hyper-parameters are selected by trials. For PGS, the Rosenbrock is added by 20,000 to ensure the search agent only encounter positive values. All numbers are rounded to keep 3 decimal places. The global maximum point of the Rosenbrock function is (1,1).

	Iterations Taken	Best Solution Found ( $\boldsymbol{\mu}^*$ )	$f(\boldsymbol{\mu}^*)$
EPGS ( $N = 3$ )	622.	(1.005, 1.013)	-0.001
PGS ( $N = 3$ )	865	(0.81, 0.698)	-0.208
STD-Homotopy	2387	(1.002, 0.998)	-0.003
ZO-SLGHd	2999	(1.181, 1.395).	-0.033
ZO-SLGHr	2999	(0.36, 0.127).	-0.41
ZO-AdaMM	1736	(-0.614, 0.582).	-6.786
ZO-SGD	45	(0.976, 1.158).	-4.189
PSO	-	(1.0, 1.0).	0.0

where  $\mathcal{C}(\mathbf{a} + \mathbf{x})_i$  denotes the predicted logit (i.e., log probability) for the  $i^{\text{th}}$  class,  $\kappa$  is a hyper-parameter that controls the certainty level of the attack,  $\lambda$  is a regularization coefficient, and  $\|\mathbf{x}\|$  denotes the  $L_1$  norm of  $\mathbf{x}$  (i.e., the square root of the sum of squares of entries in  $\mathbf{x}$ ). This loss function resembles the popular one in Carlini and Wagner (2017).

With EPGS and other compared algorithms, I perform adversarial attacks on 100 randomly selected images from each of two image datasets, the set of MNIST figures and the CIFAR-10 set. Specifically, the goal is to solve:

$$\max_{\mathbf{x}} \{-L(\mathbf{x})\}.$$

The hyper-parameters for ZO-SLGHd and ZO-SLGHr are set according to Iwakiri (2022), which performed the same task (but with a difference loss and more iterations for each trial). For ZO-AdaMM, the hyper-parameters are set according to Chen (2019) (Section 4.2). For others, the hyper-parameters are set by trials. We choose EPGS over PGS for this task since the fitness function  $-L(\mathbf{x})$  can be negative and hence EPGS is more convenient. (But note that we can modify  $-L(\mathbf{x})$  by adding a large positive constant to facilitate PGS).

### 5.3.1 MNIST

The image size in MNIST hand-written figures ([11]) is  $28 \times 28$  pixels and we down-sample it to  $14 \times 14$  to reduce the computational complexity. The classifier  $\mathcal{C}$  for MNIST is a feed-forward neural net trained<sup>7</sup> on the training images, with a classification accuracy of 96.9% on the testing images.

For each image  $\mathbf{a}_m$  that is randomly drawn from the testing dataset, where  $m \in \{1, 2, \dots, 100\}$ , we randomly generate a target label  $\mathcal{T}_m \neq \mathcal{C}(\mathbf{a}_m)$ . Then, for each algorithm, we perform an attack (i.e., experiment) of  $T_{total}$  iterations. Let  $\{\boldsymbol{\mu}_{m,t}\}_{t=0}^{T_{total}-1}$  denote all the perturbations (solutions) produced in these  $T_{total}$  iterations. We say that a perturbation  $\boldsymbol{\mu}$  is successful if the predicted log probability of the target label is at least  $\kappa = 0.01$  greater

<sup>7</sup>We use TensorFlow ([1]) for training.

than that of other classes (i.e.,  $\mathcal{C}(\mathbf{a} + \boldsymbol{\mu})_{\mathcal{T}} - \max_{i \neq \mathcal{T}} \mathcal{C}(\mathbf{a} + \boldsymbol{\mu})_i > \kappa$ ). We say that an attack is successful if the produced  $\{\boldsymbol{\mu}_{m,t}\}_{t=0}^{T_{total}-1}$  contains at least one successful perturbation. If the attack is successful, let  $\boldsymbol{\mu}_m^*$  denote the successful perturbation with the largest  $R^2$ -value among  $\{\boldsymbol{\mu}_{m,t}\}_{t=0}^{T_{total}-1}$ , and let  $T_m$  denote the number of iterations taken by the algorithm to produce  $\boldsymbol{\mu}_m^*$ . Here, the  $R^2$ -value of  $\boldsymbol{\mu}$  refers to the  $R^2$  statistic between  $\mathbf{a}$  and the perturbed image  $\mathbf{a} + \boldsymbol{\mu}$ , which is computed as  $\frac{\sum_{i=1}^m (a_i - \bar{a})^2}{\sum_{i=1}^m \mu_i^2}$ . In this formula,  $a_i$  and  $\mu_i$  ranges over all the pixels (entries) of  $\mathbf{a}$  and  $\boldsymbol{\mu}$ .

With the above notations, we construct three measures on the performances of an algorithm. One is the success rate, which refers to the ratio of successful image attacks out of the total number of attacks (100). The second measure is the average  $R^2$ , which equals  $\bar{R}^2 := \sum_{m \in \mathbb{S}} R^2(\mathbf{a}_m, \boldsymbol{\mu}_m^*) / |\mathbb{S}|$ , where  $\mathbb{S}$  denotes the set of indices of the successful attacks. The last measure is the average  $\bar{T}$  of  $\{T_m\}_{m \in \mathbb{S}}$ .

For ZO-SLGHd, ZO-SLGHr, ZO-SGD, and ZO-AdaMM, the hyper-parameters are set the same as those experiments performed in [9] (if available), since they also use these algorithms for MNIST and CIFAR-10 image attacks. For other algorithms, the hyper-parameters are selected by trials.

Table 3 reports the results of each algorithm executed for  $T_{total}$  iterations for each of the 100 images, from which we see that EPGS not only has a 100% success rate, but also is the the fastest to produce a successful perturbed image that is close to the original one. Specifically, when  $T_{total} = 500$ , EPGS outperforms other algorithms in terms of accuracy (i.e.,  $\bar{R}^2$ ) and time (i.e.,  $\bar{T}$ ). This  $\bar{R}^2$ -score of 87.10% is not far from the  $\bar{R}^2$  produced by other algorithms with 8,000 iterations.

Table 3: Targeted Adversarial Attack on 100 MNIST hand-written figures (per-image). For each image attack, the initial perturbation is set as  $\boldsymbol{\mu}_0 := \mathbf{0}$ .  $T_{total}$  denotes the total number of iterations performed for each attack. Suc. Rate denotes portion of successful attacks out of the 100 attacks.  $\bar{R}^2$  is the average of  $\{R^2(\mathbf{a}_m, \boldsymbol{\mu}_m^*)\}_{m \in \mathbb{S}}$ , where  $\mathbf{a}_m$  denotes the  $m^{th}$  original image and  $\boldsymbol{\mu}_m^*$  denotes the optimal perturbation found in the  $m^{th}$  image attack, and  $\mathbb{S}$  denotes the set of indices of the successful attacks.  $\bar{T}$  denotes the average number of iterations taken to the optimal perturbation.

	$T_{total} = 500$			$T_{total} = 8,000$		
	Succ. Rate	$\bar{R}^2$	$\bar{T}$	Succ. Rate	$\bar{R}^2$	$\bar{T}$
EPGS ( $N = 2$ )	100%	87.10%	218	100%	87.38%	7342
ZO-SLGHd	0.0	-	-	57%	91.30%	7847
ZO-SLGHr	0.0	-	-	60%	91.12%	7979
ZO-SGD	100%	74.4%	446	100%	87.93%	7594
ZO-AdaMM	100%	83.4%	483	100%	88.97%	7750
STD-Homotopy	0.0	-	-	0	-	-

### 5.3.2 CIFAR-10

The image size in CIFAR-10 dataset ([10]) is  $32 \times 32$  pixels and we down-sample it to  $16 \times 16$  to reduce the computational complexity. We train a convolutional neural net  $\mathcal{C}$  on the training images, which has a classification accuracy of 78.3% on the testing images. We perform per-image targeted adversarial attacks on 100 randomly drawn images from the testing set. The results are reported in Table 4.

The experiments are performed in the same way as for figure-MNIST and their results are reported in Table 4. Similar to the MNIST experiment, EPGS significantly outperforms

other algorithms in terms of time complexity. Especially when  $T_{total} = 500$ , the quality (i.e.,  $\bar{R}^2$ ) of its solution is much better, which is comparable to other algorithms performed for  $T_{total} = 5,000$  iterations.

Table 4: Targeted Adversarial Attack on 100 CIFAR-10 images (per-image). For each randomly drawn image  $\mathbf{a}_m$  from the testing image set, a target label  $\mathcal{T}_m \neq \mathcal{C}(\mathbf{a}_m)$  is randomly generated. The initial perturbation is set as  $\boldsymbol{\mu}_0 := \mathbf{0}$ . In the table, ‘‘Succ. Rate’’,  $\bar{R}^2$  and  $\bar{T}$  are defined in the same way as in Table 3. All numbers are rounded to keep 3 decimal places. The global maximum point of the Rosenbrock function is (1,1).

	$T_{total} = 500$			$T_{total} = 5,000$		
	Succ. Rate	$\bar{R}^2$	$\bar{T}$	Succ. Rate	$\bar{R}^2$	$\bar{T}$
EPGS ( $N = 1$ )	100%	97.58%	218	100%	97.25%	247
ZO-SLGHd	0.0	-	-	59%	99.70%	4955
ZO-SLGHr	0.0	-	-	60%	99.62%	4991
ZO-SGD	100%	-0.08%	460	100%	89.12%	4603
ZO-AdaMM	100%	79.23%	444	100%	98.43%	4927
STD-Homotopy	0.0	-	-	25%	92.74%	2008

## 6 Conclusion

In this paper, we propose the method of GSPTO for solving the global optimization problem of (1), which is featured with putting more weight on the objective’s global optimum through power transformations. Both our theoretical analysis and numerical experiments show that GSPTO is significantly faster than other homotopy methods to produce high-quality solutions. This method provides a foundation for future studies to explore more efficient ways to increase the gap between  $f(\mathbf{x}^*)$  and other values.

## References

- [1] M. Abadi, A. Agarwal, P. Barham, E. Brevdo, Z. Chen, C. Citro, G. S. Corrado, A. Davis, J. Dean, M. Devin, S. Ghemawat, I. Goodfellow, A. H., G. Irving, M. Isard, Y. Jia, R. Jozefowicz, L. Kaiser, M. Kudlur, J. Levenberg, D. Mane, R. Monga, S. Moore, D. Murray, C. Olah, M. Schuster, J. Shlens, B. Steiner, I. Sutskever, K. Talwar, P. Tucker, V. Vanhoucke, V. Vasudevan, F. Viegas, O. Vinyals, P. Warden, M. Wattenberg, M. Wicke, Y. Yu, and X. Zheng. Tensorflow: Large-scale machine learning on heterogeneous distributed systems, 2015.
- [2] A. Blake and A. Zisserman. *Visual Reconstruction*. MIT press, 1987.
- [3] J. Chen, Z. Guo, H. Li, and C. P. Chen. Regularizing scale-adaptive central moment sharpness for neural networks. *IEEE Transactions on Neural Networks and Learning Systems*, 35(5), 2024.
- [4] X. Chen, S. Liu, K. Xu, X. Li, X. Lin, M. Hong, and D. Cox. Zo-adamm: Zeroth-order adaptive momentum method for black-box optimization. *Advances in neural information processing systems*, 32, 2019.

- [5] K. Dvijotham, M. Fazel, and E. Todorov. Universal convexification via risk-aversion. In *Proceedings of the Thirtieth Conference on Uncertainty in Artificial Intelligence*, 2014.
- [6] K. Gao and O. Sener. Generalizing Gaussian smoothing for random search. In *Proceedings of the 39th International Conference on Machine Learning*, volume 162, pages 7077–7101. PMLR, 2022.
- [7] S. Ghadimi and G. Lan. Stochastic first-and zeroth-order methods for nonconvex stochastic programming. *SIAM journal on optimization*, 23(4):2341–2368, 2013.
- [8] E. Hazan, K. Y. Levy, and S. Shalev-Shwartz. On graduated optimization for stochastic non-convex problems. In *Proceedings of The 33rd International Conference on Machine Learning*, volume 48, pages 1833–1841, 2016.
- [9] H. Iwakiri, Y. Wang, S. Ito, and A. Takeda. Single loop gaussian homotopy method for non-convex optimization. In *Advances in Neural Information Processing Systems*, volume 35, pages 7065–7076. Curran Associates, Inc., 2022.
- [10] A. Krizhevsky and G. Hinton. Learning multiple layers of features from tiny images. Technical Report TR-2009, University of Toronto, 2009.
- [11] Y. LeCun, L. Bottou, Y. Bengio, and P. Haffner. Gradient-based learning applied to document recognition. *Proceedings of the IEEE*, 86(11):2278–2324, 1998.
- [12] X. Lin, Z. Yang, X. Zhang, and Q. Zhang. Continuation path learning for homotopy optimization. In *Proceedings of the 40th International Conference on Machine Learning*, volume 202, pages 21288–21311. PMLR, 2023.
- [13] M. Locatelli and F. Schoen. *Global Optimization: Theory, Algorithms, and Applications*. SIAM, Philadelphia, PA, 2013.
- [14] L. J. V. Miranda. PySwarms, a research-toolkit for particle swarm optimization in python. *Journal of Open Source Software*, 3, 2018.
- [15] H. Mobahi and J. F. III. A theoretical analysis of optimization by gaussian continuation. In *Proceedings of the AAAI Conference on Artificial Intelligence*, volume 29, pages 1205–1211, 2015.
- [16] H. Mobahi and Y. Ma. Gaussian smoothing and asymptotic convexity. Technical report, University of Illinois at Urbana-Champaign, 2012.
- [17] A. Starnes and C. Webster. Improved performance of stochastic gradients with gaussian smoothing, 2024.
- [18] L. Xiao and T. Zhang. A proximal-gradient homotopy method for the l1-regularized least-squares problem. In *Proceedings of the 29th International Conference on Machine Learning (ICML-12)*, pages 839–846, 2012.

## 7 Appendix

### 7.1 Proof to Theorem 1 for EPGS

*Proof.* Recall that for EPGS,  $f_N(\mathbf{x}_k) := \begin{cases} e^{Nf(\mathbf{x}_k)}, & \mathbf{x} \in \mathcal{S}; \\ 0, & \text{otherwise.} \end{cases}$  For any given  $\delta > 0$ , define  $V_\delta := \sup_{\mathbf{x}: \|\mathbf{x} - \mathbf{x}^*\| \geq \delta} f(\mathbf{x})$  and  $D_\delta := (V_\delta + f(\mathbf{x}^*)) / 2$ . Using this symbol, we re-write  $F_N(\boldsymbol{\mu}, \sigma)$

as

$$F_N(\boldsymbol{\mu}, \sigma) = e^{D_\delta N} G_N(\boldsymbol{\mu}, \sigma) = e^{D_\delta N} (H_N(\boldsymbol{\mu}, \sigma) + R_N(\boldsymbol{\mu}, \sigma)), \quad (7)$$

where

$$\begin{aligned} G_N(\boldsymbol{\mu}, \sigma) &:= (\sqrt{2\pi}\sigma)^{-d} \int_{\mathbf{x} \in \mathbb{R}^d} e^{-ND_\delta} f_N(\mathbf{x}) e^{-\frac{\|\mathbf{x}-\boldsymbol{\mu}\|^2}{2\sigma^2}} d\mathbf{x}, \\ H_N(\boldsymbol{\mu}, \sigma) &:= (\sqrt{2\pi}\sigma)^{-d} \int_{\mathbf{x} \in B(\mathbf{x}^*; \delta)} e^{-ND_\delta} f_N(\mathbf{x}) e^{-\frac{\|\mathbf{x}-\boldsymbol{\mu}\|^2}{2\sigma^2}} d\mathbf{x}, \\ R_N(\boldsymbol{\mu}, \sigma) &:= (\sqrt{2\pi}\sigma)^{-d} \int_{\mathbf{x} \notin B(\mathbf{x}^*; \delta)} e^{-ND_\delta} f_N(\mathbf{x}) e^{-\frac{\|\mathbf{x}-\boldsymbol{\mu}\|^2}{2\sigma^2}} d\mathbf{x}, \end{aligned}$$

where  $B(\mathbf{x}^*; \delta) := \{\mathbf{x} \in \mathbb{R}^d : \|\mathbf{x} - \mathbf{x}^*\| < \delta\}$ .

We derive an upper bound for  $\left| \frac{\partial R_N(\boldsymbol{\mu}, \sigma)}{\partial \mu_i} \right|$ . For any  $\boldsymbol{\mu} \in \mathbb{R}^d$ ,

$$\begin{aligned} \left| \frac{\partial R_N(\boldsymbol{\mu}, \sigma)}{\partial \mu_i} \right| &\leq \frac{1}{(\sqrt{2\pi})^d \sigma^{d+2}} \int_{\mathbf{x} \notin B(\mathbf{x}^*; \delta)} |x_i - \mu_i| e^{-\frac{\|\mathbf{x}-\boldsymbol{\mu}\|^2}{2\sigma^2}} e^{-ND_\delta} f_N(\mathbf{x}) d\mathbf{x} \\ &\leq \frac{1}{(\sqrt{2\pi})^d \sigma^{d+2}} \int_{\mathbf{x} \notin B(\mathbf{x}^*; \delta)} |x_i - \mu_i| e^{-\frac{\|\mathbf{x}-\boldsymbol{\mu}\|^2}{2\sigma^2}} e^{N(f(\mathbf{x}) - D_\delta)} d\mathbf{x} \\ &\leq \frac{1}{(\sqrt{2\pi})^d \sigma^{d+2}} \int_{\mathbf{x} \notin B(\mathbf{x}^*; \delta)} |x_i - \mu_i| e^{-\frac{\|\mathbf{x}-\boldsymbol{\mu}\|^2}{2\sigma^2}} e^{N(V_\delta - D_\delta)} d\mathbf{x} \\ &\leq \frac{e^{N(V_\delta - D_\delta)}}{(\sqrt{2\pi})^d \sigma^{d+2}} \int_{\mathbf{x} \in \mathbb{R}^d} |x_i - \mu_i| e^{-\frac{\|\mathbf{x}-\boldsymbol{\mu}\|^2}{2\sigma^2}} d\mathbf{x} \\ &\leq e^{N(V_\delta - D_\delta)} \left( \prod_{j \neq i} \frac{1}{\sqrt{2\pi}\sigma} \int_{x_j \in \mathbb{R}} e^{-\frac{(x_j - \mu_j)^2}{2\sigma^2}} dx_j \right) \\ &\quad \cdot \frac{1}{\sqrt{2\pi}\sigma^3} \int_{x_i \in \mathbb{R}} |x_i - \mu_i| e^{-\frac{(x_i - \mu_i)^2}{2\sigma^2}} dx_i \quad (8) \\ &= e^{N(V_\delta - D_\delta)} \frac{1}{\sqrt{2\pi}\sigma^3} \int_{y \in \mathbb{R}} \sqrt{2}\sigma |y| e^{-y^2} d(\sqrt{2}\sigma y), \quad y := \frac{x_i - \mu_i}{\sqrt{2}\sigma}, \\ &= e^{N(V_\delta - D_\delta)} \frac{\sqrt{2}}{\sqrt{\pi}\sigma} \cdot 2 \int_0^\infty y e^{-y^2} dy, \quad y := \frac{x_i - \mu_i}{\sqrt{\pi}\sigma}, \\ &= e^{N(V_\delta - D_\delta)} \frac{\sqrt{2}}{\sqrt{\pi}\sigma} \cdot \int_0^\infty e^{-y^2} dy^2, \\ &= e^{N(V_\delta - D_\delta)} \frac{\sqrt{2}}{\sqrt{\pi}\sigma} \cdot \int_0^\infty e^{-z} dz, \\ &= \frac{\sqrt{2} e^{N(V_\delta - D_\delta)}}{\sqrt{\pi}\sigma} \end{aligned}$$

where the third line is because  $\|\mathbf{x} - \mathbf{x}^*\| \geq \delta \Rightarrow f(\mathbf{x}) \leq V_\delta$ , and the fifth line is by the separability of a multivariate integral.

Since  $f$  is continuous, for  $\epsilon_\delta := f(\mathbf{x}^*) - D_\delta > 0$  (because  $V_\delta < f(\mathbf{x}^*)$ ), there exists  $\delta' \in (0, \delta)$  such that whenever  $\|\mathbf{x} - \mathbf{x}^*\| \leq \delta'$ ,

$$f(\mathbf{x}) \geq f(\mathbf{x}^*) - \epsilon_\delta = D_\delta > V_\delta. \quad (9)$$



Using this result, we derive a lower bound for  $\left| \frac{\partial H_N(\boldsymbol{\mu}, \sigma)}{\partial \mu_i} \right|$  when  $\|\boldsymbol{\mu}\| \leq M$  and  $|\mu_i - x_i^*| > \delta$ .

$$\begin{aligned}
\left| \frac{\partial H_N(\boldsymbol{\mu}, \sigma)}{\partial \mu_i} \right| &= \frac{1}{(\sqrt{2\pi})^d \sigma^{d+2}} \int_{\mathbf{x} \in B(\mathbf{x}^*; \delta)} |x_i - \mu_i| e^{-ND_\delta} f_N(\mathbf{x}) e^{-\frac{\|\mathbf{x} - \boldsymbol{\mu}\|^2}{2\sigma^2}} d\mathbf{x} \\
&= \frac{1}{(\sqrt{2\pi})^d \sigma^{d+2}} \int_{\mathbf{x} \in B(\mathbf{x}^*; \delta)} |x_i - \mu_i| e^{-\frac{\|\mathbf{x} - \boldsymbol{\mu}\|^2}{2\sigma^2}} e^{N(f(\mathbf{x}) - D_\delta)} d\mathbf{x}, \text{ since } B(\mathbf{x}^*; \delta) \subset \mathcal{S}, \\
&\geq \frac{1}{(\sqrt{2\pi})^d \sigma^{d+2}} \int_{\mathbf{x} \in B(\mathbf{x}^*; \delta')} |x_i - \mu_i| e^{-\frac{\|\mathbf{x} - \boldsymbol{\mu}\|^2}{2\sigma^2}} e^{N(f(\mathbf{x}) - D_\delta)} d\mathbf{x} \\
&\stackrel{\text{by (9)}}{\geq} \frac{1}{(\sqrt{2\pi})^d \sigma^{d+2}} \int_{\mathbf{x} \in B(\mathbf{x}^*; \delta')} (\delta - \delta') e^{-\frac{\|\mathbf{x} - \boldsymbol{\mu}\|^2}{2\sigma^2}} d\mathbf{x} \\
&\geq \frac{1}{(\sqrt{2\pi})^d \sigma^{d+2}} \int_{\mathbf{x} \in B(\mathbf{x}^*; \delta')} (\delta - \delta') e^{-\frac{M^2}{\sigma^2}} e^{-\frac{\|\mathbf{x}\|^2}{\sigma^2}} d\mathbf{x}, \quad \|\mathbf{x} - \boldsymbol{\mu}\|^2 \leq 2(\|\mathbf{x}\|^2 + \|\boldsymbol{\mu}\|^2), \\
&\geq (\delta - \delta') e^{-\frac{M^2}{\sigma^2}} V(\delta', d, \sigma)
\end{aligned} \tag{10}$$

where the first equality is implied by the fact that  $x_i - \mu_i$  does not change sign as  $\mathbf{x}$  travels in  $B(\mathbf{x}^*; \delta)$  (this fact is because of  $|\mu_i - x_i^*| > \delta$ ), and

$$V(\delta', d, \sigma) = \frac{1}{(\sqrt{2\pi})^d \sigma^{d+2}} \int_{\mathbf{x} \in B(\mathbf{x}^*; \delta')} e^{-\frac{\|\mathbf{x}\|^2}{\sigma^2}} d\mathbf{x}.$$

The positive number  $N_{\delta, \sigma, M}$  is constructed by solving the following inequality for  $N$ , which involves the two bounds in (8) and (10).

$$\frac{\sqrt{2} e^{N(V_\delta - D_\delta)}}{\sqrt{\pi} \sigma} < (\delta - \delta') e^{-\frac{M^2}{\sigma^2}} V(\delta', d, \sigma).$$

The solution of this inequality is

$$N > \frac{\ln \left( \frac{\sqrt{\pi}}{\sqrt{2}} (\delta - \delta') e^{-\frac{M^2}{\sigma^2}} V(\delta', d, \sigma) \right)}{V_\delta - D_\delta},$$

where  $V_\delta - D_\delta < 0$  and the numerator is negative for sufficiently large  $M > 0$ . Therefore, whenever

$$N > N_{\delta, \sigma, M} := \max \left\{ 0, \frac{\ln \left( \frac{\sqrt{\pi}}{\sqrt{2}} (\delta - \delta') e^{-\frac{M^2}{\sigma^2}} V(\delta', d, \sigma) \right)}{V_\delta - D_\delta} \right\},$$

we have

$$\left| \frac{\partial R_N(\boldsymbol{\mu}, \sigma)}{\partial \mu_i} \right| < \frac{\sqrt{2} e^{N(V_\delta - D_\delta)}}{\sqrt{\pi} \sigma} < (\delta - \delta') e^{-\frac{M^2}{\sigma^2}} V(\delta', d, \sigma) < \left| \frac{\partial H_N(\boldsymbol{\mu}, \sigma)}{\partial \mu_i} \right|. \tag{11}$$

When  $N > N_{\delta, \sigma, M}$ ,  $\|\boldsymbol{\mu}\| \leq M$ , and  $\mu_i > x_i^* + \delta$ ,

$$\begin{aligned}
\frac{\partial G_N(\boldsymbol{\mu}, \sigma)}{\partial \mu_i} &= \frac{\partial H_N(\boldsymbol{\mu}, \sigma)}{\partial \mu_i} + \frac{\partial R_N(\boldsymbol{\mu}, \sigma)}{\partial \mu_i} \\
&= \frac{1}{(\sqrt{2\pi})^k \sigma^{k+2}} \int_{\mathbf{x} \in B(\mathbf{x}^*; \delta)} (x_i - \mu_i) e^{-\frac{\|\mathbf{x} - \boldsymbol{\mu}\|^2}{2\sigma^2}} e^{N(f(\mathbf{x}) - D_\delta)} d\mathbf{x} + \frac{\partial R_N(\boldsymbol{\mu}, \sigma)}{\partial \mu_i} \\
&= - \left| \frac{\partial H_N(\boldsymbol{\mu}, \sigma)}{\partial \mu_i} \right| + \frac{\partial R_N(\boldsymbol{\mu}, \sigma)}{\partial \mu_i} \\
&\stackrel{\text{by (11)}}{<} - \left| \frac{\partial R_N(\boldsymbol{\mu}, \sigma)}{\partial \mu_i} \right| + \left| \frac{\partial R_N(\boldsymbol{\mu}, \sigma)}{\partial \mu_i} \right| \\
&= 0,
\end{aligned} \tag{12}$$

where the third line is because the integrand of the first term is always negative in the integration region.

On the other hand, when  $N > N_{\delta, \sigma, M}$ ,  $\|\boldsymbol{\mu}\| \leq M$ , and  $\mu_i < x_i^* - \delta$ ,

$$\begin{aligned}
\frac{\partial G_N(\boldsymbol{\mu}, \sigma)}{\partial \mu_i} &= \frac{\partial H_N(\boldsymbol{\mu}, \sigma)}{\partial \mu_i} + \frac{\partial R_N(\boldsymbol{\mu}, \sigma)}{\partial \mu_i} \\
&= \left| \frac{\partial H_N(\boldsymbol{\mu}, \sigma)}{\partial \mu_i} \right| + \frac{\partial R_N(\boldsymbol{\mu}, \sigma)}{\partial \mu_i} \\
&\stackrel{\text{by (11)}}{>} \left| \frac{\partial R_N(\boldsymbol{\mu}, \sigma)}{\partial \mu_i} \right| - \left| \frac{\partial R_N(\boldsymbol{\mu}, \sigma)}{\partial \mu_i} \right| \\
&= 0.
\end{aligned} \tag{13}$$

Then, (12) and (13) imply the result in the theorem since  $\frac{\partial G_N(\boldsymbol{\mu}, \sigma)}{\partial \mu_i}$  and  $\frac{\partial F_N(\boldsymbol{\mu}, \sigma)}{\partial \mu_i}$  share the same sign (see Eq. (7)).  $\square$